A Displacement-Current Double Closed-Loop Control Algorithm for BPMSS

Wen-tao Shan, Zhen-hua Han

Abstract—**In view of the temperature rise, noise and vibration between the rotor and the support bearings under the high-speed rotating state of the PMSMS, the bearingless technology is proposed for avoiding the contact between the rotor and the support bearings and achieving stable compensation of the motorized spindles under high-speed running state. Based on the modeling method of ordinary bearingless motors, mathematical models of the BPMSS and simulation experiments are carried out. At the same time, the variable structure PID is used in the displacement controller to optimize the displacement control of the rotor. The results prove the feasibility of bearingless technology on permanent magnet synchronous motorized spindles. The magnetic levitation system largely avoids the contact between the rotor and the support bearings, which can solve the noise and vibration problems of the rotor when running at high speeds. Variable structure PID has a stronger control effect on rotor displacement control than ordinary PID control strategy.**

Index Terms—**Bearingless motorized spindles; Stable suspension; Variable structure PID; Bearingless technology; Displacement control**

I. Introduction

With the development of power electronics and modern control techniques, the theory of bearingless permanent magnet synchronous motors and related technologies have been continuously developed and improved. The bearingless motor was initially proposed by Kant Krishan [1], which revealed the relationship between the numbers of windings of the motors. Raghu [2] first proposed BPMSM, which laid the foundation for the research of BPMSM. Barletta [3] applied vector control to the bearingless motor and developed an experimental prototype. In 2016, German scholar G. Bergmann provided design guidelines for bearingless motors, which laid the foundation for the future design of BPMSM [4]. Many scholars have summarized the development of bearingless motors and proposed many novel control methods on the original basis [5-7]. Although the design methods and applications for bearingless motors continue to increase, the application of bearingless technology to high-speed motorized spindles has not yet become widespread. Although the structure of ordinary bearingless motors is different from that of motorized spindles, the principle of electromagnetic torque generated by bearingless motors is basically the same as that of motorized spindles, and some aspects of bearingless motors have advantages that motorized spindles do not have in high-speed and high-precision situations. Therefore, it is necessary to study bearingless motorized spindles, which combine the two kinds. Especially when the rotor vibration problem under the current high-speed operation of the motorized spindle has not been effectively solved, it is highly important to study the application of bearing less technology in the high-speed motorized spindle.

The bearingless permanent magnet synchronous motorized spindle (BPMSS) not only has the excellent performance of traditional motorized spindles but also has the function of rotor magnetic suspension. It can avoid the damage caused by friction from rotor and support bearings under high-speed rotating state and increases the critical speed of the motorized spindles. Based on the research of BPMSS, this research work studies the operation of surface-mounted BPMSS at high-speed running state [8]. The bearingless motorized spindle is a complex system with strong coupling of machine, electric, magnetic and heat. It is an important requirement to achieve efficiently decoupling between electromagnetic torque and radial suspension force.

At present, current control technology becomes an interesting research themes for scholars at home and abroad. The current control strategies for traditional permanent magnet synchronous motorized spindles are as follows: magnetic field directional control, Maximum Torque Per Ampere (MTPA), $\cos\varphi$ =1 control, constant flux linkage control and so on. Focusing on the suspension force control, there are also many control strategies such as double closed-loop displacement-current control, fuzzy PID control of suspension force, and direct control of radial displacement [9-11]. This paper analyzes and derives the mathematical model of BPMSS, employs the rotor field orientation control and the displacement-current double closed-loop control to simulate the running state of BPMSS. The improved displacement PID controller uses variable structure PID (VSPID) control strategy to solve the problems of slow response and high overshoot [12]. At last, high-quality drive is realized under high-speed running condition.

II. The Mathematical Model of BPMSS

The stator windings of the bearingless permanent magnet synchronous motorized spindle have a complicated electromagnetic relationship with the rotor permanent magnet.

Manuscript received November 8, 2023; revised May 24, 2024.

This work was supported in part by the National Natural Science Foundation of China under Grant 52005229, Qing Lan Project of JiangSu Province under Grant KYQ20004 and Major Project of Natural Science Research in Universities of JiangSu under Grant 19KJA510001.

Wen-tao Shan is a Professor of Jiangsu University of Technology, Jiangsu, Changzhou, China (corresponding author: 0086-519-86953205; fax: 0086-519-86953205; E-mail: shanwentaoedu@yeah.net).

Zhen-hua Han is a Professor of Jiangsu University of Technology, Jiangsu, Changzhou, China. (E-mail: doo_kwonbaik@yeah.net).

There are many nonlinear factors in it. Therefore, it is of great difficulty to build a precise and accurate mathematical model of the BPMSS. Aiming at accurately describing its mathematical model, the following assumptions are made:

(1) The core reluctance, hysteresis losses and eddy current losses of the motors in the permanent magnet synchronous motorized spindle are ignored;

(2) The magnetic saturation phenomenon is ignored;

(3) The stator and rotor windings of BPMSS are completely symmetrical. The rotor and stator surfaces are smooth in suppose. There are no cogging effects. The magnetic potential of each phase of the rotor and stator is sinusoidally distributed in space;

(4) When the BPMSS is in a stable operation condition, the inductive electrodynamic potential in the stator windings inside the spindle is a sine wave;

(5) The space phase axis, phasor time axis, α axis, displacement sensor center line are all coincident, then the β axis is ahead of the α axis by 90 °spatial angle;

(6) To generate stable levitation force, $P_M=P_B\pm1$, the current frequency is equal, and the number of the torque winding pole and the suspension winding pole is 4 and 2 respectively.

A. The Torque Mathematical Model

The electromagnetic torque model of a BPMSS is similar to that of a traditional motor [13]. The torque winding u and ψ equations in the d-q axis are calculated to equations (1) and (2).

$$\begin{cases} u_{Md}=\dfrac{d\psi_{Md}}{dt}-\omega_e\psi_{Mq}+R_M i_{Md} \\ u_{Mq}=\dfrac{d\psi_{Mq}}{dt}+\omega_e\psi_{Md}+R_M i_{Mq} \end{cases} \tag{1}$$

$$\begin{cases} \psi_{Md}=L_{Md}i_{Md}+\psi_f \\ \psi_{Mq}=L_{Mq}i_{Mq} \end{cases} \tag{2}$$

In this research work, a surface-mounted bearingless motorized spindle is studied. Here, stator inductance $L_{Md}=L_{Mq}=L_M$, R_M is the rotor resistance. ω_e is electrical degree velocity of the rotor. ψ_f is the flux linkage produced by the permanent magnet motorized spindle. i_{Md} and i_{Mq} stand for the components of the torque current under the d-q axis.

From above, it can be deduced that under constant power conversion, the input torque T_e of the high-speed motorized spindle is derived just as showed in equation (3).

$$T_e=P_M(\psi_{Md}i_{Mq}-\psi_{Mq}i_{Md}) \tag{3}$$

The mechanical motion equation of the motorized spindle is derived in following equation.

$$T_e-T_L=J\frac{d\omega_r}{dt} \tag{4}$$

Here P_M is the numbers of pole pairs, J is the moment of inertia of the motorized spindle, and ω_r is the mechanical angular velocity of the rotor.

B. The Suspension Force Model

It can be known from ordinary bearingless motors that when the stator winding satisfies $P_M=P_B\pm1$, the stable radial suspension force is produced by the combined action of α axial force and β axial force [14-16]. As shown in Fig1 (a) and 1(b):

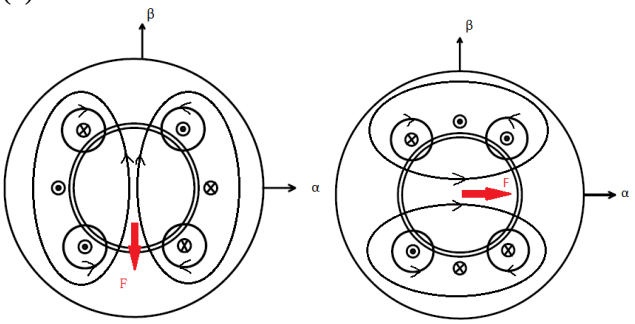

(a) α axial force (b) β axial force

Fig 1. The sketch map of α and β axial force

The purpose of adding suspension force in the stator windings is mainly to improve the distribution state, and then stimulate out Maxwell force so that the rotor axis can be designed right at the center of the stator. The electromagnetic torque of the motorized spindle is still produced by the Lorentz force of the torque windings, which is the same as the ordinary motor. The force direction of the two figures is exactly 90 degrees different in angle. In Figure 1(a), the generated flux direction of the levitation winding on the α-axis is to the right. The left side magnetic flux and that generated by the torque winding are mutually inhibited. In contrast, the fluxes on the right side are superimposed by each other, resulting in a positive levitation force. In Fig 1(b), the mechanism of generated suspension force of the β axis is similar to that of the α axis (the direction of the suspension force depends on the current direction of the suspension winding). The specific working principle can be seen from the above two figures and the actual conversion relationship between flux linkage and torque can be realized in this process. When the rotor displacement in the two mutually perpendicular α and β axis directions can be effectively controlled, the eccentricity and vibration of the rotor can be effectively suppressed to realize the stable operation of the motorized spindle.

Considering the rotor eccentricity, and mutual-inductance current between the rotor and stator. Through the derivation of mathematical model, the flux linkage matrix of the motorized spindle under the d-q coordinate system can be derived in following matrix equation (5).

$$\begin{bmatrix} \psi_{Md} \\ \psi_{Mq} \\ \psi_{Bd} \\ \psi_{Bq} \end{bmatrix}=\begin{bmatrix} L_M & 0 & Mx & -My \\ 0 & L_M & My & Mx \\ Mx & My & L_B & 0 \\ -My & Mx & 0 & L_B \end{bmatrix}\begin{bmatrix} i_{Md}+I_f \\ i_{Mq} \\ i_{Bd} \\ i_{Bq} \end{bmatrix} \tag{5}$$

Therefore, the magnetic co-energy equation of the two sets of windings is derived just as showed in the following equation (6), this matrix equation contains four current components and four flux components. In equation (6), the

flux linkages of the four dimensions are taken into account, besides, the current of *d-q* axis is considering together.

$$W_{\mathrm{m}}=\frac{1}{2}\begin{bmatrix} i_{Md}+I_f & i_{Mq} & i_{Bd} & i_{Bq}\end{bmatrix}\begin{bmatrix}\psi_{Md}\\ \psi_{Mq}\\ \psi_{Bd}\\ \psi_{Bq}\end{bmatrix} \tag{6}$$

The radial electromagnetic force of the rotor can be obtained by the partial derivative of the magnetic co-energy, as shown in equation (7)

$$\begin{cases} F_{\mathrm{x}}=\dfrac{\partial W_m}{\partial x}\\ F_y=\dfrac{\partial W_m}{\partial y}\end{cases} \tag{7}$$

According to the literature [17], the controllable suspension force model of BPMSS obtained by simplifying is expressed as the formula (8)

$$\begin{bmatrix}F_{\mathrm{x}}\\ F_y\end{bmatrix}=M\begin{bmatrix} i_{Md}+I_f & i_{Mq}\\ i_{Mq} & -i_{Md}-I_f\end{bmatrix}\begin{bmatrix}i_{Bd}\\ i_{Bq}\end{bmatrix} \tag{8}$$

Here M stands for the mutual inductance coefficient, and I_f stands for the equivalent exciting current of the permanent magnet motor.

Similarly, the radial controllable suspension force formula (9) is calculated through Maxwell tensor method [18-19].

$$\begin{cases} F_x=(k_M-k_L)(i_{Bd}\psi_{Md}+i_{Bq}\psi_{Mq})\\ F_y=(k_L-k_M)(i_{Bq}\psi_{Md}-i_{Bq}\psi_{Mq})\end{cases} \tag{9}$$

Where Maxwell force constant $k_M=(\pi P_M P_B L)/(12lr\ \mu_0 N_1 N_2)$, and Lorentz force constant $k_L=(3P_M N_2 k_2)/(4rk_1 N_1)$. L is the mutual inductance value. k_1 and k_2 are the coefficients of two sets of torque windings, respectively.

According to the modern control theory, it is known that when the rotor is eccentric, the rotor will also experience unilateral magnetic pull forces F_{sx} and F_{sy}, which are proportional to the eccentric displacement. They are an inherent force of the system [20], and their expression is equation (10). The system is mainly composed of sliding mode controller, the leading angle magnetic weakening controller and current regulator. The speed error n_e is used as the input signal of the sliding mode controller. By virtue of the advantages of sliding mode control, such as insensitivity to disturbance and parameters and fast response time, the speed tracking performance of the proposed control system is improved greatly and it is output as the input signal of the next processing. Through calculating, the set values of stator current of direct axis and quadrature axis can be obtained, and then, two different reference values and the actual stator current values are obtained, and the output is used as the input signal of current regulator. When fuzzy control strategy is adopted, russification steps can be decreased. However, when the Markowitz model is used for deducing the result. The fuzzy PID controller outputs the running speed of the motorized spindle in real time, The current value and the change rate obtained by two different fuzzy control observers can be sent to the inverter controller of the next process together, so that the current control is more accurate. The fuzzy control rule table of the control system is established by two parameters. In order to make the current tracking more accurate, the double closed-loop control of position and speed is set up. In this scheme, sliding mode control is adopted to optimize the output performance of the drive system and imropve the anti-jamming ability. The speed range of PMSMS is extended by the leading angle weak magnetic control, and the current PI controller is used to ensure that the stator current can track the instruction value quickly and accurately.

$$\begin{cases} F_{sx}=k_x x\\ F_{sy}=k_y y\end{cases} \tag{10}$$

Where radial displacement stiffness parameters $k_x=k_y=(k\pi rlB^2)/(\mu_0\delta_0)$; x and y stand for values of the radial displacements under *d-q* rotating coordinate system, respectively; k stands for the attenuation factor.

In general, the rotor is subjected to its own gravity and the disturbance force perpendicular to the direction of gravity when the motor spindle is working, then, through coordinate transformation of some columns, the motion equation of permanent magnet synchronous motorized spindle in the static coordinate system is finally derived.

$$\begin{cases} m\dfrac{\mathrm{d}^2\alpha}{dt^2}=f_d+F_\alpha-F_{s\alpha}\\ m\dfrac{d^2\beta}{dt^2}=mg+F_\beta-F_{s\beta}\end{cases} \tag{11}$$

Where f_d is the disturbance force, and m is the rotor mass. The control variable method should be adopted in the trial adjustment processing, and each parameter should be adjusted systematically to make the control result tend to the ideal state.

III. The Control System Model

In this simulation, the torque winding current is controlled by rotor field orientation with $i_{Md}^*=0$. The torque calculation module in the controller can be obtained by simplifying equation (3). Then, the signal obtained by SVPWM modulation is used to control the inverter output current to the motorized spindle.. The displacement controller (i.e., the dotted line) uses PID regulator and variable structure PID regulator to compare the control effect. The current regulators all use PI controllers, where the force/current conversion module can be obtained by simplifying the controllable suspension force equation (8). Finally, because of the built-in dual current loop that the output speed of motorized spindle is more continuous and smooth. The required current is also output by SVPWM to complete the control requirements. Finally, the drive control system model is shown in Figure 2.

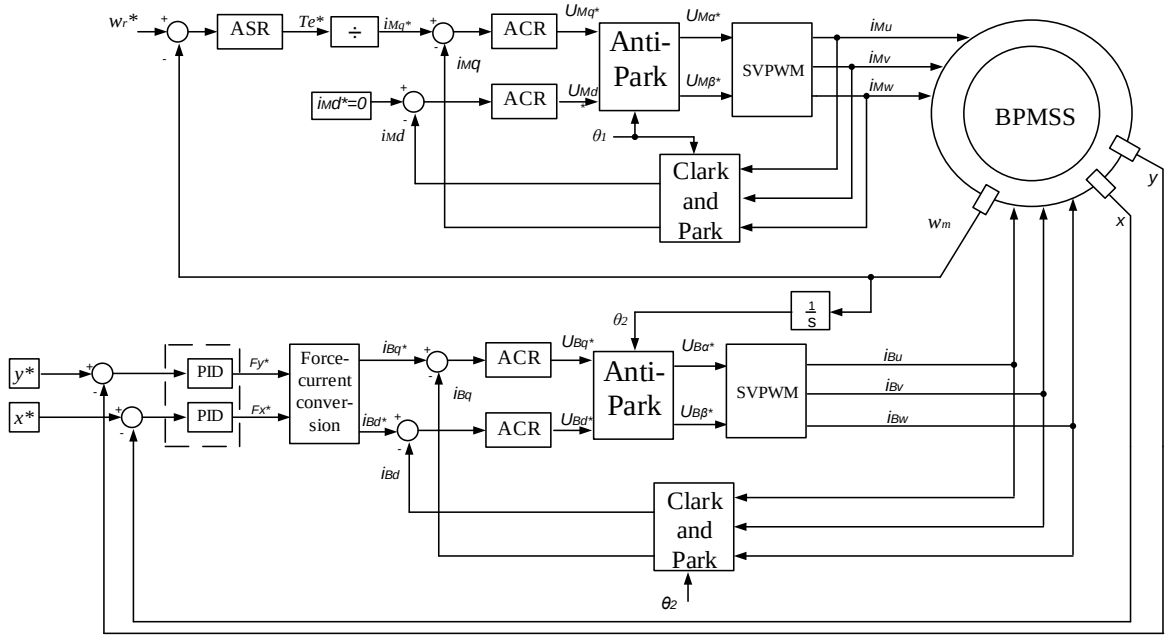

Fig 2. The drive control system model of BPMSS

Among them, VSPID regulator transforms the three coefficients in the traditional PID regulator so that it can change the model structure and key parameters of the controller in real time with the change of the deviation e(t). The formula used for variable structure PID is shown in formula (12)

$$u(e,t) = K_P(e)\cdot e(t) + K_i(e)\cdot\int e(t)dt + K_d(e)\cdot\frac{de(t)}{dt} \quad (12)$$

Where $K_{\mathrm{p}}(e) = a_p + b_p(1-e^{-c_p|e(t)|})$, $K_{\mathrm{i}}(e)=a_i e^{-c_i|e(t)|}$, $K_{\mathrm{d}}(e) = a_d - b_d(1-e^{-c_d|e(t)|})$; a_p, b_p, c_p, a_i, c_i, a_d, b_d and c_d are all positive numbers.

The change curve of the proportional coefficient is shown in Fig 3. The scaling factor K_p follows the same trend as the error e(t) and achieves a larger value when the error is larger (maximum value is a_p+b_p). As the error decreases, its value is continuously reduced, improving the response speed, suppressing the overshoot amount well and ensuring system stability.

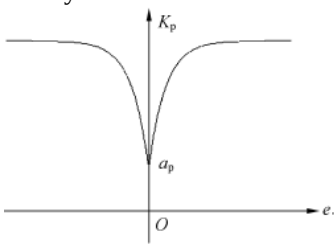

Fig 3. K_p change curve

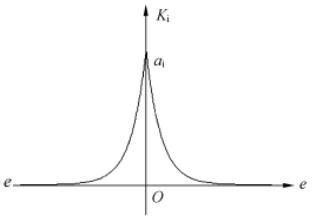

Fig 4. Ki change curve

The curve of the integration factor K_i in Figure 4 shows that K_i is a very small value tending to zero at large errors. This law can prevent oscillation while reducing overshoot and adjustment time. When the error is small, K_i will be near the maximum a_i to eliminate the steady-state error.

Fig 5 shows the trend of the differential coefficient. In the case of large initial errors, the differential coefficients will obtain smaller values as a way to achieve faster response times. When the system reaches steady state, K_d obtains a larger value to maintain the stable output for the system.

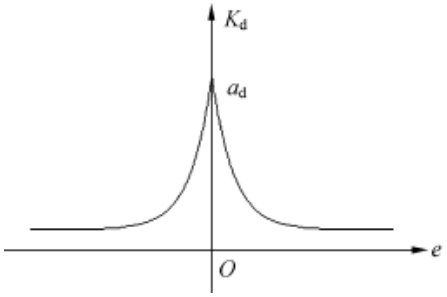

Fig 5. K_d change curve

From the variation of the three parameters of the variable structure PID, it is clear that the use of variable structure PID control can reduce the requirement of system model accuracy, and the control objectives of the system can be achieved within a certain range.

The simulation time is 1.4 seconds. The given speed n* is 10,000*r/min*. From Fig 6, we can see that the motorized spindle firstly reaches a stable running speed at 0.72*s*, and the error remains within 1*r/min*. The load torque suddenly changes to 10N m at 1.0*s*. The partially enlarged view in Figure 4.1 shows that the speed returns to its steady state value in a very short time. Fig 7 also shows the torque variation curve, with small fluctuations in torque and a quick arrival at the given value when a sudden load is applied. Due to the use of PID control, there is a small amount of overshoot.

TABLE I
MAIN PARAMETERS OF THE MOTORIZED SPINDLE

Parameter Name	Values	Parameter Name	Values
Torque winding resistance R_M/Ω	0.15	Suspension winding resistance R_B/Ω	1.86
Torque winding inductance L_M/mH	2.8	Suspension winding inductance L_B/mH	2.8
Rotational inertia J/(kg•m^2)	0.015	Air gap length δ_0/mm	0.5
Permanent magnet chains ψ_f/Wb	0.114	Auxiliary bearing-rotor clearance δ_1/mm	0.3
DC voltage U/V	540		

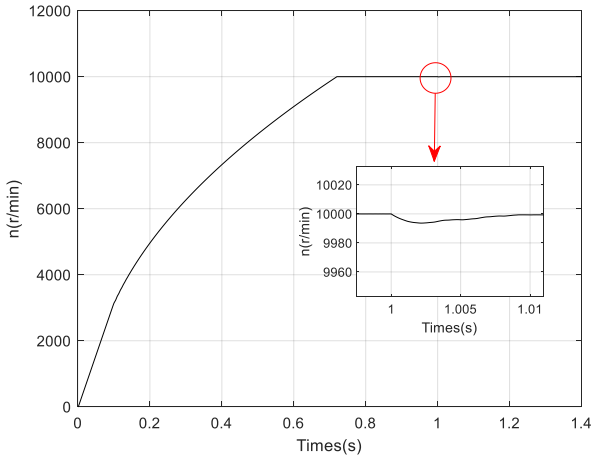

Fig 6. BPMSS speed curve under the traditional PI controller

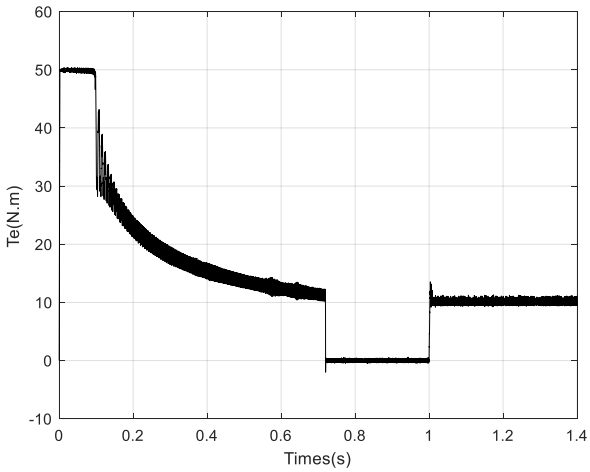

Fig 7. BPMSS torque curve under the traditional PI controller

Fig 8 and Fig 9 show the displacement curves of the rotor in α and β axes respectively. Initial disturbance force f is 0N, and the initial position of the rotor is x_0=-0.1mm and y_0=-0.3mm. The control system uses 0.3s to adjust the rotor position so that it can stably converge to $\pm$0.002mm. The disturbance force changes to 10N at 1.0s. In the lower right corner of the pictures, we have laid out a local enlarged view to facilitate the reader to more clearly observe the characteristics of the two control strategies that α-axis displacement gradually stabilizes within -0.001~0mm. β-axial displacement is stable within 0.0019~0.0028mm. The rotor position deviation is much smaller than the minimum gap δ_1. From the partial enlargement of the upper half of the rotor α-axis displacement, Figure 10, it can be seen that the variable structure PID is better than the ordinary PID. The overshoot is reduced nearly 17.5% by ordinary PID. The partially enlarged view of β-axis displacement is also similar to the α-axis, so it will not be shown here. Besides, the response time of proposed system is also sharply reduced, which effectively improves the processing efficiency. Through comparison, it can be found that using the proposed control strategy in this paper can achieve better results in response time, overshoot, adjustment time and other aspects, which is also conducive to the realization of high-speed and high-precision processing. However, when the advanced PID controller is generally adopted, there will occur some problems such as large current fluctuation and insufficient anti-interference ability. To solve the negative effects of PID controller, a nonlinear disturbance rejection controller is proposed for solving this problem.

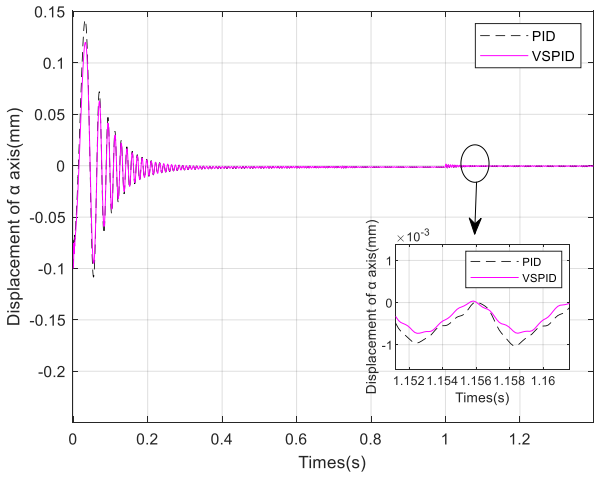

Fig 8. α axial displacement

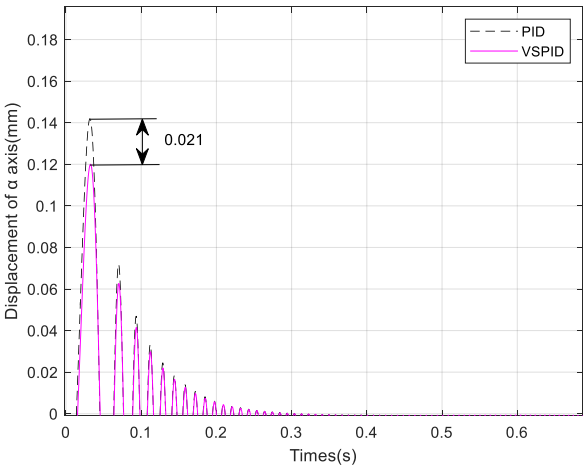

Fig 9. A partially enlarged view of the upper half of the α axial displacement

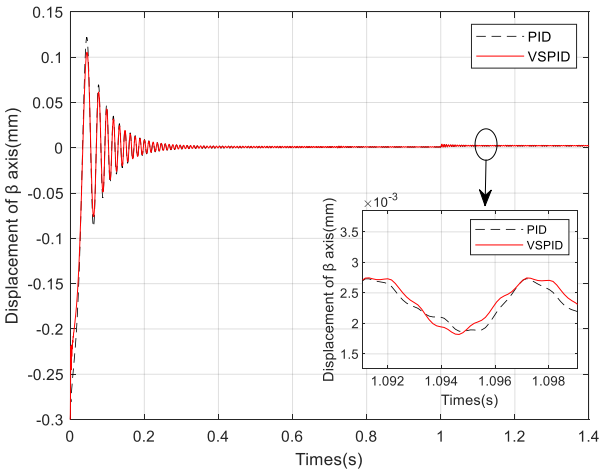

Fig 10. β axial displacement

Fig 11 shows the trajectory of the rotor in space. Due to the large initial torque current, the rotor displacement is greatly affected. As the torque current decreases, the rotor's center approaches the stator's center in a spiral manner. At the same time, it can be seen more clearly in the space plane that variable structure PID adjustment can make the rotor displacement reach the steady state value faster. At last, the motorized spindle will realize its stable running operation.

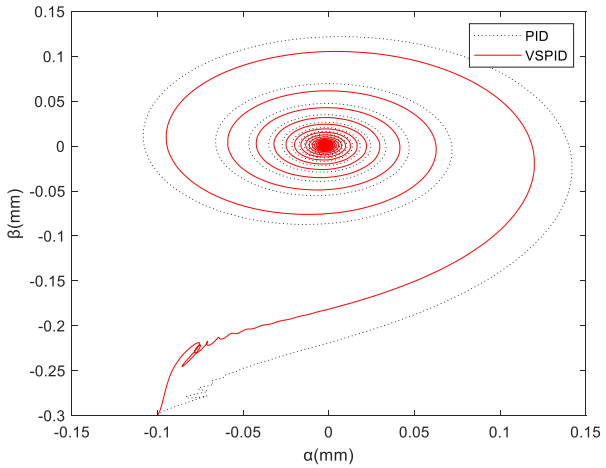

Fig 11. The rotor shaft center trajectory

IV. Conclusion

This article applies BPMSS control technology into high-speed motorized spindles. The feasibility of a high-speed BPMSS has been demonstrated through simulation experiments. The suspension force control method chooses the traditional displacement-current double closed-loop control. After using this control strategy, the control current generated by SVPWM can get stable suspension, and greatly improve the output performance of the motorized spindle. Meanwhile, the rotor displacement is adjusted using a variable structure PID and good results are obtained. However, the displacement stiffness coefficients and mutual inductance coefficients in the model need to be analyzed by finite element analysis to obtain accurate values. It laid the foundation for the establishment of a more accurate model and the application of intelligent control theory to achieve more precise control requirements.

References

[1] K. Krishan, A novel bearingless interior permanent magnet slice motor driven blood pump. *Mechatronics*. vol. 90, no. 4, pp. 547-588, Jan. 2023.

[2] Raghu K, and Prameela Kumari N. Direction of Arrival Estimation by Employing Intra-block Correlations in Sparse Bayesian Learning Through Covariance Model, *Engineering Letters*, vol. 31, no.1, pp82-92, 2023.

[3] N. Barletta, R. Schoeb. Principle and application of a bearingless slice motor. In: *Proceedings of 9th International Symposium on Magnetic Bearings*, 2021, Kanazawa, Japan, pp. 313-318.

[4] Wei-Guo Zhang, Qing Zhu, Hong-Juan Zheng, Lin-Lin Gu and Hui-Jie Lin, "Economic and Optimal Dispatch Model of Electricity, Heat and Gas for Virtual Power Plants in Parks Considering Low Carbon Targets," *Engineering Letters*, vol. 31, no.1, pp. 93-104, 2023.

[5] Ying Xu, Huangqiu Zhu. Development of Bearingless Permanent Magnet Synchronous Motor System and Key Technologies. *Proceedings of the CSEE*. vol. 39, no. 10, pp. 2994-3003, Oct.2022.

[6] Yang Z, Lu C, Sun X, et al. Study on Active Disturbance Rejection Control of a Bearingless Induction Motor Based on an Improved Particle Swarm Optimization-Genetic Algorithm. *IEEE Transactions on Transportation Electrification*, vol. 34, no. 12, pp. 123-135. Feb. 2021.

[7] Bu W, Lu P, Lu C, et al. Independent Inverse System Decoupling Control Strategy of Bearingless Induction Motor. *Recent Advances in Motorizedal & Electronic Engineering*. vol. 13, no. 7, pp. 1001-1009. Jan. 2020.

[8] Xin Tong. High-gain Output Feedback Control for Linear Stepping Motor Based on Fuzzy Approximation. *IAENG International Journal of Computer Science*, vol. 50, no.3, pp. 910-914, 2023.

[9] Huangqiu Zhu, Jianfei Yuan, Jintao Ju. A novel single winding structure and closed loop control of the suspension force vector of bearingless permanent magnet synchronous motors. *Energies*. vol. 9, no. 5, pp. 377-382. Nov.2021.

[10] Zhijian Qiu, Zhiquan Deng, Xiaolin Wang. A study on independent control of the bearingless permanent magnet synchronous motor. *Proceedings of the CSEE*, 2006, 26(1): pp. 115-119.

[11] He Zhu, Hongchao Xing, Jinfu Zhu, and Ping Zhang. Design of Fuzzy Gait Control Algorithm for Multi-legged Hydraulic Robot. *IAENG International Journal of Computer Science*, vol. 50, no.3, pp. 1042-1049, 2023.

[12] Bin Zhang, Hongwen Li, Lihong Guo, Haoran Meng, Jianli Wang, Yumei Yin.Application of variable structure PID in velocity control for large telescope. *Optics and Precision Engineering*. Vol. 18, no. 7, pp.1614-1622. Feb. 2022.

[13] Huangqiu Zhu, Ying Qin, Jintao Ju, Fayu Li. General model of BPMSM based on flux linkage interaction analysis. *Journal of Vibration and Shock*. vol. 34, no. 17, pp. 192-198. Nov. 2015.

[14] Bichels J. The bearingless motorizedal machine. Proc. Int. Symp. Magn. Suspension. Technol. NASA Langley Res. Center, Hampton, 2021.

[15] Huangqiu Zhu, Tao Zhang. Finite Element Analysis for Bearingless Permanent Magnet-type Synchronous Motors. *Proceedings of the CSEE*. vol.26, no.3, pp. 138-140, Jan. 2022.

[16] Oshima M, Yamaida K, Chiba A. An improved control method of buried-type IPM bearingless motors considering magnetic saturation and magnetic pull variation. *IEEE Trans on Energy Conversion*, vol. 19, no. 3, pp. 569-575, Mar. 2021.

[17] Qiu Z, Dai J, Yang J, Zhou X, Zhang Y. Research on rotor eccentricity compensation control for bearingless surface-mounted permanent-magnet motors based on an exact analytical method. *IEEE Trans Magn*. vol. 51, no. 4, pp. 1-4. Jul. 2015.

[18] Ke Li, Xiaodong Sun, Zebin Yang. Radial force model of bearingless permanent magnet synchronous motors. *Bearing*, 2014(12): pp.10-13.

[19] Lei Huang, Huangqiu Zhu. Research Status and Development Trend of Bearingless Permanent Magnet Synchronous Motor. *Micromotors*. vol. 52, no. 8, pp. 94-98. Nov. 2019.

[20] Kazuki Ota, and Hideki Katagiri. Demand Forecasting of Bento Considering the Product Popularity Estimation for Multiple Types of Bento Menus Using a Bayesian Rating System. Lecture Notes in Engineering and Computer Science: *Proceedings of the International MultiConference of Engineers and Computer Scientists*. 2023, 5-7 July, 2023, Hong Kong, pp. 7-13.

Wen-tao Shan received his PHD degree in Mechanical Engineering from Chongqing University in 2013. Moreover, his main research direction is intelligent control algorithm for Bearingless Permanent Magnet Synchronous Motorized Spindle, test and detection technology for motorized spindles. Now, he serves as a Professor in Jiangsu University of Technology.

Zhen-hua Han received his PHD degree in Mechanical Engineering from Chongqing University in 2019. Moreover, his main research direction is precision transmission design. Now, he serves as a lecturer in Jiangsu University of Technology.